Chapter 3

Large scale turbulence cascade in two nearby spiral galaxies[1]

In this chapter, we present the new H I observations of two spiral galaxies. We use the visibility moment estimator to estimate the column density and line of sight velocity power spectra. Based on the result of this investigation, we comment on the origin and properties of the large scale turbulence in these galaxies.

3.1 Sample selection

The visibility moment estimators(VME) discussed earlier assume that the galaxy of interest has a nearly face-on thin disc. A typical external spiral galaxy's disc is expected to have an arbitrary inclination angle with respect to the line of sight direction. The nearly face-on disc ensures that the angular separation we observe can be directly related to length scales on the face of the disc. Further, considering a tilted ring model for the galaxy's large scale dynamics, the inclination, as well as the position angle is required to be smoothly varying with the radial separation from the galaxy's centre (galactocentric distance). The VME

[1]Part of the work presented in this chapter is originally published in Nandakumar and Dutta (2020)

Source	D Mpc	$i_{\rm HI}$ deg	PA deg	R_{25} (kpc)	H I extent $\rm B_{maj} \times B_{min}$(kpc)	SFR $\rm M_\odot yr^{-1}$	$\rm M_{HI}$ $10^8 M_\odot$	$\rm M_{dy}$ $10^{11} M_\odot$
NGC 5236	4.77	24	225	10.9	42×33	2.52	17.0	2.6
NGC 6946	5.9	33	243	9.8	60×43	4.76	41.5	7.3

Table 3.1 Some parameters of the selected galaxies. Columns 1-9 gives 1) Name of the galaxy, 2) Distance to the galaxy in Mpc, 3) Average H I inclination angle, 4) Position angle, 5) Optical radius R_{25} in kpc, 6) H I extent in kpc which is major and minor axis at the level of column density brightness of 10^{19}atoms cm^{-2}, 7) Star Formation Rate, 8) H I mass, 9) Dynamical Mass. These values are obtained from the following references: Bottinelli and Gouguenheim (1973); de Blok et al. (2008); Ianjamasimanana et al. (2015); Leroy et al. (2008); Pierce (1994); Radburn-Smith et al. (2011); Schmidt et al. (1992); Walter et al. (2008)

is originally discussed in Dutta (2016). They used models of galaxies to show that the VME for the power spectrum of the line of sight velocity fluctuations has less uncertainty for inclination angle between 15^0 and 40^0. Hence, the VME should be used only for the galaxies with disc inclination angles in this range. We also restrict to galaxies for which the position angle and inclination do not vary much with radius. The rotation curves of 18 galaxies from the THINGS survey along with the radial variation of position angle and the inclination angle are presented in de Blok et al. (2008). We analyse their data to search for galaxies samples whose tangential velocity component of receding and approaching parts of the disc is almost similar. Hence, we make sure that the disc of selected galaxies is nearly flat and with not much variation in inclination and position angle with radius. To see the connection between the turbulence at larger scale cascade that is mostly observed in external galaxies and small scale cascade that is mostly probed in our Galaxy, we need to measure the density and velocity fluctuations over at least two decades of length scale ranging $\sim$ 10 kpc or higher to $\sim$ 100 pc or lower for sample galaxies. Hence we selected galaxies with having considerably large H I extent.

Based on the above criteria we selected two galaxies NGC 5236 and NGC 6946 to investigate turbulence in their ISM. NGC 5236 also known as M 83 is a barred spiral

galaxy. The galaxy has a nearly face-on disc with an average inclination angle of 24° (Tilanus and Allen, 1993; Walter et al., 2008). The tilted ring rotation curve model from earlier H I studies shows that the inclination and position angles vary monotonically with galactocentric distance (Huchtmeier and Bohnenstengel, 1981). NGC 6946 is a bright late-type spiral galaxy. This galaxy has well defined spiral structures and is found to have H I structures like holes and high velocity gas (Boomsma et al., 2008; Kamphuis and Sancisi, 1993). From the rotation curve estimation by de Blok et al. (2008), the systematic velocity of NGC 6946 is fairly constant with radius. The H I profile width at 20% of the peak intensity for NGC 5236 and NGC 6946 are $\sim$ 270 km sec^{-1} and 240 km sec^{-1} respectively. Table 3.1 summarizes the following properties of these galaxies: (1) Galaxy name, (2) distance to the galaxy, (3) H I inclination angle, (4) position angle, (5) optical radius (R_{25}), (6) H I major and minor axes, (7) star formation rate, (8) the total H I and (9) dynamical mass. The inclination and position angle given are disc averaged values used. The optical radius R_{25} is the radius where the B band surface brightness is at the level of 25 magnitude arcsec^{-2}. The H I extent is defined as the major and minor axis at the level of the column density of 10^{19} atoms cm^{-2}.

Walter et al. (2008) have used different array configurations of the VLA to observe 34 nearby galaxies including NGC 5236 and NGC 6946. NGC 5236 is observed with the VLA hybrid configurations BnA, CnB and DnC for about 12, 2 and 20 hours respectively. NGC 6946 was observed using B,C,D configurations of VLA for 10.5, 1.75 and 0.25 hours respectively. Velocity resolution corresponding to each channel for both galaxies in the THINGS survey is 2.6 km sec^{-1}. Dutta et al. (2013) estimated specific intensity fluctuation power spectra of these two galaxies using THINGS data, where both of them are obeying a power law. For the galaxy NGC 5236, the slope of the power law is -1.9 ± 0.2 from 800 pc to 7.5 kpc and NGC 6946 has a slope -1.6 ± 0.1 in length scale ranging from 300 pc to 4 kpc. Though estimations are indicating the presence of large scale energy cascade in these

Galaxy	Telescope	Date of Observation	No of Channels	Bandwidth (MHz)	On source time (hrs)
NGC 5236	GMRT	June, July 2018	4096	12	11.5
NGC 6946	VLA A array	May-June 2018 Oct 2019	2048	4	11.6

Table 3.2 Different parameters regarding the H I observations of two galaxies is given in this table. Galaxy name, Telescope used for observation, date of observation, bandwidth and channel number, total integration time on source are given in each column.

galaxies, owing to the rather small signal to noise in visibility at baseline values larger than 10 kλ in the THINGS data set, these results have the following limitations. The smallest length scale we probe here is still larger than the expected size of the smallest of the WNM clouds, we could not estimate the slope and amplitude of the velocity power spectrum significantly. Hence these galaxies need to be observed freshly with better dynamic range and spectral resolution for estimation of density or velocity fluctuation power spectra at length scales ranging over the scales of the galaxies.

3.2 Observations and data analysis

The VME requires observations with high signal to noise over a large range of baselines as well as high spectral resolution. Following is the detailed description of observations of two galaxies and following data reduction procedure. Table 3.2 tabulate the different parameters of observations of two galaxies.

3.2.1 NGC 5236

NGC 5236 was observed with the uGMRT[2] on 02, 03 June and 31 July 2018 for a total observation time of 14 hours at the L band. We used a total of 4096 channels over a 12 MHz bandwidth centred at the redshifted frequency of the galaxy. The larger bandwidth was

[2]upgraded Giant Meterwave Radio Telescope (Gupta et al., 2017)

chosen to accurately model the continuum emission. Each channel in the data corresponds to a velocity resolution of 0.6 km sec^{-1}, adequate to study the turbulent velocity fluctuations in the galactic disc. Primarily, we processed the observations of each day separately. We used the standard tasks in classic AIPS[3] to edit the data for radio frequency interference and primary calibration. The calibrated data from each day is then combined using the AIPS task DBCON and exported to a FITS[4] file. The half power beam width of the uGMRT at the L-band is $25'$. Given the large H I extend of NGC 5236, it is required to use modern deconvolution algorithms to estimate the continuum model for this galaxy. We used the CASA[5] for modelling the continuum and self-calibration. CASA task 'tclean' provides better options for imaging in a large field of view observations. The continuum model is subtracted from the visibilities in each channel by UVSUB algorithm using CASA tasks 'ft' and 'uvsub'.

3.2.2 NGC 6946

We observed NGC 6946 using the A array configuration of VLA in two observation cycles in 2018 and 2019 in L-band. A total of 14 hours of observation was broken down into separate 2 hours long observation blocks and carried out in total of seven days during the two cycles. The total bandwidth of the observation was 4 MHz (~ 845 km sec^{-1}). A total of 2048 channel in this bandwidth results in a spectral resolution of ~ 0.4 km sec^{-1}. The H I Galactic foreground emission from our Galaxy is also lying within the same frequency bandwidth we are observing, hence both calibrators and the target source's frequency spectra are contaminated with the same. Hence it was required to carry out in-band frequency switching procedure additionally during the observation. The primary calibration and flagging were carried out in each observation block separately

[3]AIPS: Astronomical Image Processing System, NRAO
[4]FITS: Flexible Image Transport System
[5]CASA: Common Astronomy Software Application, NRAO

using CASA. The frequency switching is incorporated in bandpass calibration during the primary calibration. Thereafter self-calibration and continuum subtraction procedures were done on the combined data from all days. Note that we flagged the channels which are contaminated by the emission from our Galaxy.

3.2.3 Combining with the THINGS data

The angular extents of both NGC 5236 and NGC 6946 are rather large and it barely fits in the primary beam of the GMRT and VLA respectively at the L band. Further, at low baselines, the GMRT baseline coverage is rather poor resulting in less sensitivity at large scales. Similarly for VLA, the smallest baseline measurable in A array configuration corresponds to an angular scale 1.3" which is very small compared to galactic size. We use the THINGS UV data to improve on the sensitivity and baseline coverage at smaller baselines for both galaxies. We start with the THINGS data with primary calibration[6] and use the same procedure as discussed above to produce the continuum subtracted UV data for further analysis. The GMRT and VLA observations are separately processed with our power spectrum estimators. Fig 3.1 shows the optical images of two galaxies with H I contours overplotted on it.

3.3 Implementation of the visibility moment estimator

Dutta and Nandakumar (2019) show that the scale-dependent quantities like the power spectrum of the specific intensity fluctuations can be estimated unbiasedly directly in the visibility domain. They also show that the large scale structure of the galaxy, like the $\langle M_j(\vec{\theta})\rangle$ can be estimated from the reconstructed image. We estimate the first and second moment of visibility $V_0(\vec{U})$ and $V_1(\vec{U})$ from the calibrated and continuum subtracted

[6]We are indebted to Prof. Fabian Walter for providing us with the calibrated uvdata.

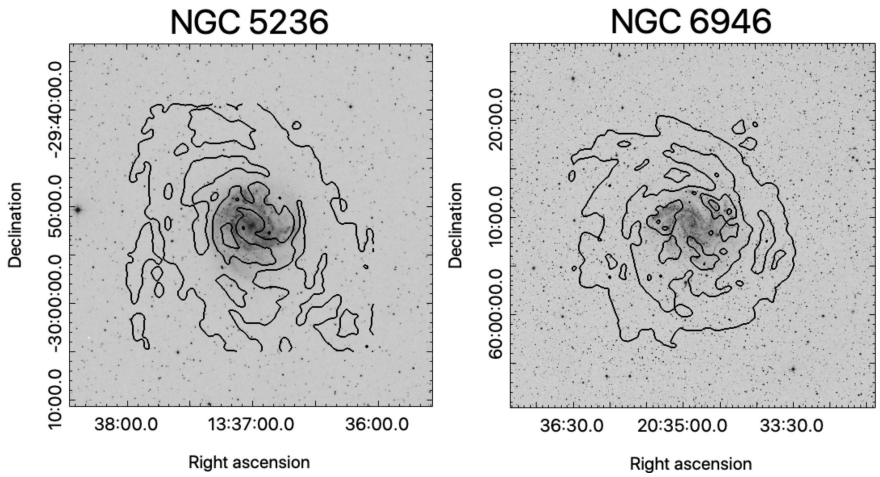

(a) NGC 5236 (b) NGC 6946

Fig. 3.1 The SDSS optical (blue-band) images of the two galaxies are shown in background grey scale. The H I column density maps from THINGS survey are plotted with black contours. The contour levels are at $(1,\ 5,\ 10,\ 15,\ 20) \times 10^{20}$ atoms cm^{-2} for both the galaxies. Optical images are obtained from the public domain of Skyview survey metadata (Lasker et al., 1990). The x-axis is the right ascension given in hh:mm:ss (hour, minute, second) and the y-axis is declination given in dd:mm:ss (degree, arc minute, arc second).

visibilities. Since in a radio interferometric observation, the visibilities are sampled at random positions in the baseline plane, the visibility moments are estimated only at the sampled baseline positions. Note that the baselines for a given antenna pair at a given time are different for different frequency channels. However, owing to the small fractional bandwidth, the difference in our observation is rather small and can be ignored. We generate position-position-frequency data cube from the continuum subtracted visibilities and use it to estimate $M_j(\vec{\theta})$. A Gaussian kernel $L(\vec{\theta}) = \frac{1}{2\pi\theta_0^2}\exp(-\mid \vec{\theta} \mid^2 /2\theta_0^2)$ with $\theta_0 = 5'$ is used to estimate the $\langle M_0(\vec{\theta})\rangle$ and $\langle M_1(\vec{\theta})\rangle$. For a Gaussian approximation to $M_j(\vec{\theta})$, this value of θ_0 gives a column density of 10^{19} atoms cm^{-2} at $4 \times \theta_0$. We calculate the discrete Fourier transform of the M_j multiplied by the primary beam of the corresponding telescopes at the sampled baseline positions to estimate $W_j(\vec{U})$. The

corresponding $X_j(\vec{U})$ are estimated at the sampled baseline positions by direct subtraction of the $W_j(\vec{U})$s from the visibility moments.

Dutta and Bharadwaj (2013) and Dutta et al. (2013) used a visibility based power spectrum estimator to calculate the power spectrum of H I intensity fluctuations from nearby galaxies. The power spectrum estimator uses visibility correlation at nearby baselines to reduce possible bias that may arise from the measurement noise. In this work, we use a similar visibility correlation estimator for quantity Q_0. To estimate the power spectrum at a baseline $\vec{U}$, we first correlate every pair of X for all baselines within a circular region of radius D in the baseline plane centred at $\vec{U}$. The value of D needs to be smaller than the inverse of the angular extent of the galaxy (see eqn (2.38) and eqn (2.41)). We then average the correlations in each circular regions (as stated above) in annular bins in the baseline plane. To calculate the column density power spectrum $P_{\rm HI}(U)$, we proceed to estimate the denominator in eqn (2.38) in the following way. We use the properties of Fourier transform, $\int \mathrm{d}\vec{U}' \mid W_0(\vec{U}') \mid^2 = \int \mathrm{d}\vec{\theta}' \mid \langle M_0(\vec{\theta}') \rangle A(\vec{\theta}) \mid^2$ and use the latter for estimation of the denominator. The real part of the ratio of the annular averaged quantity discussed above to the calculated denominator gives estimates of the $P_{\rm HI}$ at baselines larger than $1/\theta_0$. The visibility correlation at nearby baselines reduces the amplitude of the correlation with respect to the correlation at the same baselines (Dutta et al., 2013). The effect of this bias is larger if a relatively larger value is chosen for D. The imaginary part of the same quantity measures a bias in the above estimator that may arise if D is chosen to be large. Hence, the ratio of the real to the imaginary part at each baseline gives a diagnostics on the choice of D. We check the ratio of the real to the imaginary part at each baseline and only consider points where the ratio is more than 3. Dutta (2011) discussed the errors in such estimators. The errors we quote here are calculated using the same method assuming that the error in the estimate of the denominator in eqn (2.38) is negligible.

To estimate the velocity power spectrum P_v we proceed the following way. At a baseline $\vec{U}$, we choose all other baselines $\vec{U}'$ within a circular region of radius D as before and calculate the function $H(\vec{U},\vec{U}')$ using our estimate of the $P_{\rm HI}$ and W_1. For each of these pair of baselines, we also calculate $X_1(\vec{U}')^* X_1(\vec{U})$ and subtract $H(\vec{U},\vec{U}')$ from it. The real part of the azimuthal average of this quantity normalised by the $\int \mathrm{d}\vec{U}' \mid W_0(\vec{U}') \mid^2$ gives estimates of the velocity power spectrum at baselines larger than $1/\theta_0$. Errors in these estimators are calculated in a similar way as done for the column density power spectrum assuming the errors in W_1 are negligible. Further, we also observed that the errors in the column density power spectra are rather small and do not contribute much to the errors in the velocity power spectrum.

3.4 Results

We process the different observations of two galaxies as discussed in section 3.3 separately for power spectrum analysis. The H I angular extent of both the galaxies are more or less similar and a value of $\theta_0 \sim 25'$ corresponds to a baseline of ~ 0.15 kλ [7]. Conservatively, for the baseline range > 0.3 kλ we may use eqn (2.38) and eqn (2.41) to estimate the column density and velocity power spectra respectively. We use $D = 0.075$ kλ for our analysis. The H I emission for both galaxies spans over a velocity range of about 300 km sec^{-1}. In NGC5236, for the GMRT observations, we choose the central 200 channels that have a comparatively higher signal to noise. These correspond to a velocity width of 120 km sec^{-1} out of the total line width $\sim$ 300 km sec^{-1}. Similarly for NGC6946, we choose central 400 channels that correspond to 165 km sec^{-1}. Note that restricting our analysis only to the central channels does not affect the measurement of the power spectra, it only limits the measurements of the column density and velocity at a limited part of the baseline plane. This was used as an advantage by Dutta et al. (2010) to

[7] kλ means 1000 wavelengths.

estimate the power spectra of different parts of the galaxy NGC 4254. We follow the procedure highlighted in section 3.3 to estimate the column density power spectra and the corresponding errors for all observations. The empty circles in Figure 3.2 shows the measurements of the azimuthally averaged values of $P_{\rm HI}$ as a function of baselines. Note that the power spectrum is a real quantity, however, the right hand side of eqn (2.38) can have a non zero imaginary part. If the imaginary part of this expression is smaller than the real part, the expression estimates the power spectrum. We use the measurement points for which the real parts are more than the imaginary parts.

We use the central 90 and 64 channels of the THINGS data of NGC 5236 and NGC 6946 respectively, with a higher signal to noise for the power spectrum analysis. The estimated values of the column density power spectrum are shown in the two panels with black filled circles in Figure 3.2. The power spectrum values for both the GMRT and VLA observations are scaled down by a factor of 10 from their original values for presentation purposes.

Clearly, at baselines smaller than $\sim\ 0.8$ kλ the GMRT observation of NGC 5236 does not provide any measurement of the power spectrum. Similarly due to the A array configuration of VLA, new observed data of NGC 6946 also lacks any measurement less than $\sim\ 2$ kλ. Note that the A array configuration of VLA is purely meant for observing the smallest scale structures in the sky with high spatial resolution, while other B, C and D are meant to capture the large scale structures in the sky. The THINGS data gives better estimates of the power spectrum at lower baselines, however, at larger baselines, the estimates are dominated by measurement noise in both galaxies.

We fit a power law of form $A\,U^{\alpha}$ to the data and estimate the best fit parameters for both the THINGS and the new observations separately. Note that owing to the effect of the window function, the power law fit can be done to a minimum baseline U_{min}. Similarly, at very large baselines, the noise becomes dominant and the imaginary part of the eqn (2.38)

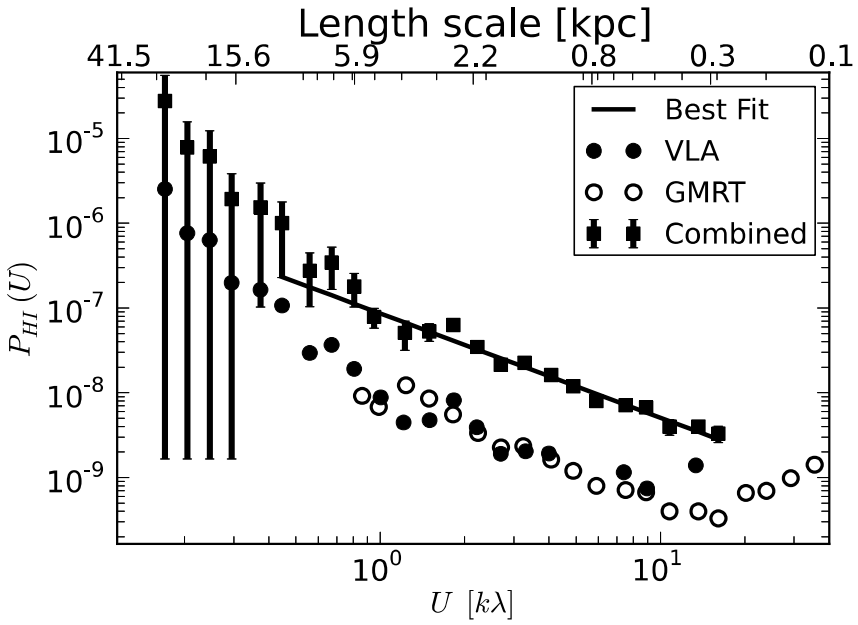

(a) NGC 5236

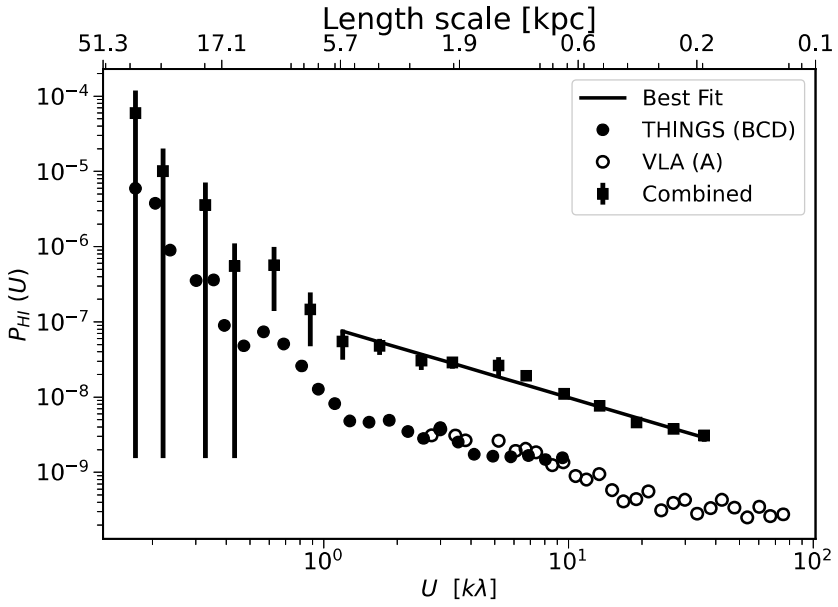

(b) NGC 6946

Fig. 3.2 Column density power spectrum of NGC 5236(top) and NGC 6946(bottom) as a function of baseline. The corresponding length scales are also shown in the top margin. The black solid circles correspond to the measurement of the column density from the THINGS data alone. The black open circles correspond to measurement using only the uGMRT/eVLA observations. These two sets of points are scaled down by a factor of ten for display purpose. The black solid squares with error bars give the power spectra measurements combining the old THINGS and the new observations. A best fit power law to the combined measurement is shown using black solid lines.

	$P_{\rm HI}(\vec{U})$	$P_{\rm HI}(\vec{U})$	$P_{\rm HI}(\vec{U})$	$P_v(\vec{U})$
NGC 5236				
Telescope	THINGS	GMRT	Combined	GMRT
$A(\times 10^4)$	4.0 ± 0.8	5.0 ± 0.6	4.0 ± 0.4	88 ± 9*
α	-1.2 ± 0.3	-1.24 ± 0.07	-1.23 ± 0.06	-1.91 ± 0.08
reduced χ^2	1.7	1.1	1.1	1.1
$U_{min}(k\lambda)$	0.6	0.9	0.4	0.9
$U_{max}(k\lambda)$	3	16	16	16
$R_{min}(kpc)$	1.4	0.3	0.3	0.3
$R_{max}(kpc)$	9	5	11	6
NGC 6946				
Data	THINGS	VLA	Combined	Combined
$A(\times 10^4)$	0.46 ± 0.08	2.3 ± 0.5	0.67 ± 0.09	59 ± 13*
α	-0.93 ± 0.1	-1.09 ± 0.08	-0.96 ± 0.05	-1.81 ± 0.07
reduced χ^2	0.7	1.2	1.1	1.2
$U_{min}(k\lambda)$	1	3	1	1
$U_{max}(k\lambda)$	6	36	36	35
$R_{min}(kpc)$	1	0.15	0.16	0.17
$R_{max}(kpc)$	6	3	5	6

Table 3.3 Result of power law fit ($P = AU^{\alpha}$) to the column density ($P_{\rm HI}$) and velocity (P_v) power spectra. The power law amplitude (A) at one steradian, best fit slope α, $1-\sigma$ errors associated with the fit, the reduced χ^2 values and the range of fit in baselines and corresponding length scale ranges are shown. The density power spectra fit is shown for the THINGS data, the new observation data and the combined power spectra. The velocity power spectra results are only from the GMRT data for NGC 5236 and from combined data for NGC 6946. The amplitudes for the density spectra are scaled by a factor of 10^4 and have a unit of steradian. *The amplitude of the velocity spectra is not scaled and is given in (km sec^{-1})^2 steradian.

becomes larger than the real part. This restricts the fit to a largest baseline of U_{max}. We first approximately decide the U_{min} and U_{max} and then estimate the reduced χ^2 value for the fit. We change the values of U_{min} and U_{max} such that the reduced χ^2 is close to unity. The final choice of these two baselines are based on the value of reduced χ^2 that is near to unity. This procedure is followed in general for all the power spectra shown here. The range of fit in baselines, the corresponding length scales at the galaxy, the value of the reduced chi-square and the best fit values with $1-\sigma$ errors for the parameters A and α are given in Table 3.3.

It is to be noted that since we choose the channels with a higher signal to noise only to estimate the power spectra, the effective angular extent of the galaxy reduces. As discussed earlier, this results in a more stringent choice in the value of D and may bias the visibility moment estimator near to the inverse of the effective angular scale. To avoid this bias we only use the estimates with the real part three times or more than the imaginary part. Black squares with error bars show the combined power spectrum from the earlier THINGS observations and the new estimates (there is no scaling of these values). We use the following procedure to combine the power spectra from the two observations. We first choose the union of the baseline ranges over which the individual power spectra are estimated and divide it into N_{bin} equal logarithmic bins. We average the estimate of the power spectra in each bin after weighting them by the corresponding errors. The error bars in each bin are calculated by taking the root mean square of the individual error estimates in the given bin. It can also be seen clearly in Figure 3.2 that at smaller baselines the power spectra (solid squares) deviate from the power law behaviour and excess power is measured. This is the region where $\mid \vec{U} \mid < 1/\theta_0$ and the convolution effect in eqn (2.37) is important. We find that the combined power spectra assume a power law between the baseline range of $0.4-16$ kλ for NGC 5236 and $1.19-36$ kλ for NGC 6946. The best fit value of A and α to the combined power spectra for NGC 5236

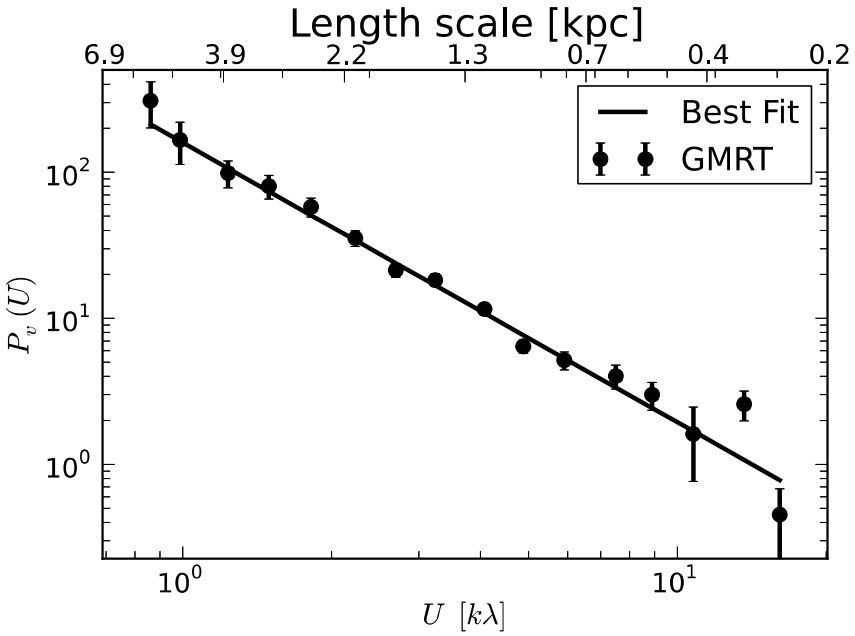

(a) NGC 5236

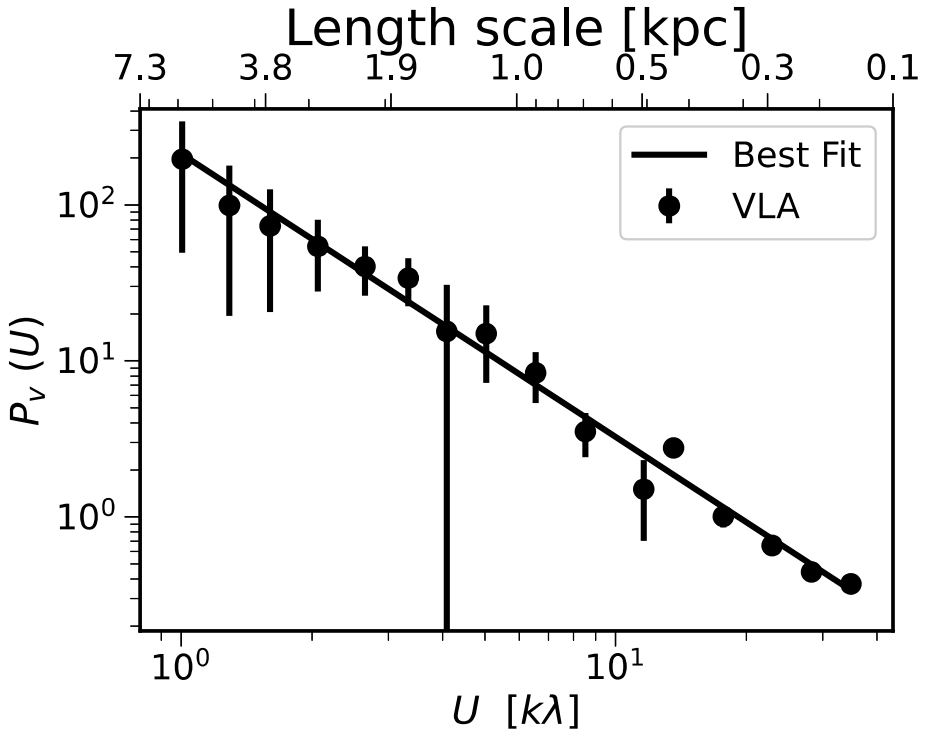

(b) NGC 6946

Fig. 3.3 The turbulent velocity power spectrum of NGC 5236(top) and NGC 6946(bottom) as a function of baseline. The corresponding length scales are also shown in the top margin. The black solid circles with error bars correspond to the measurement from the uGMRT observations in NGC 5236 and combined observations for NGC 6946. A best fit power law to the combined measurement is shown using black solid lines.

are $(4.0 \pm 0.4) \times 10^{-4}$ steradian and -1.23 ± 0.06 respectively with the goodness of fit given by the reduced chi-square of 1.1 (see Table 3.3). Similarly for NGC 6946, value of A and α are $(6.7 \pm 0.9) \times 10^{-5}$ steradian and -0.96 ± 0.05 respectively. The amplitudes mentioned here are at the baseline of one wavelength. These are the first determinations of the column density power spectra over almost two decades of length scales for external spiral galaxies.

We use a similar procedure to estimate the power spectrum of the line of sight velocity fluctuations using the new observations. For NGC 5236, the THINGS observation has a relatively low velocity resolution of 2.6 km sec^{-1} compared to what we would have required to estimate the velocity power spectrum. Moreover, the GMRT observations have significant measurement points in a smaller baseline (upto $\sim 800\lambda$), which is adequate for the measuring velocity fluctuations in the corresponding length scales. Hence we do not use the THINGS data for NGC 5236. In the case of NGC 6946, the VLA A array observation with high velocity resolution has limited measurement at baseline < 3 kλ. In this case, we use THINGS data with the new VLA A array observation and combine the estimates to get the velocity power spectrum. The combination of two velocity power spectra for NGC 6946 is done following the same procedure as for the column density power spectrum. The power spectrum estimates along with the error bars are shown with black circles in Figure 3.3 for both galaxies.

3.5 Discussion

In this work, we measure H I column density and line of sight velocity power spectra of two spiral galaxies NGC 5236 and NGC 6946 using visibility moment estimators with the GMRT and the VLA observations. The power spectra are estimated over more than one decade of length scales that ranges from ~ 160 pc to 11 kpc on the galactic disc. These

Type of Turbulence	$P_{\rm HI}(\vec{U})$	$P_v(\vec{U})$	References
Kolmogorov	-	$-5/3$	Kolmogorov (1941)
Burger's	-	-2	Burgers (1948)
Weizsacker	$4\alpha - 2$	$-5/3 - 4\alpha/3$	Fleck (1996)
Solenoidal	-0.78 ± 0.06	-1.86 ± 0.05	Federrath et al. (2009)
Compressive	-1.44 ± 0.23	-1.94 ± 0.05	Federrath et al. (2009)
NGC 5236	-1.23 ± 0.06	-1.91 ± 0.08	This work
NGC 6946	-0.96 ± 0.05	-1.81 ± 0.07	This work

Table 3.4 Power spectral slope for density and velocity for different theoretical models of turbulence and simulations. All the spectral slopes are given for what is expected for turbulence in the thin disk as the case for this observational result. Here α is the compressibility factor.

are the first measurements of the column density power spectra on such large length scale range and the first measurement of the velocity power spectra in external spiral galaxies.

In an earlier work, Dutta et al. (2013) reports that for 10 out of the 18 external spiral galaxies from the THINGS survey, the slope of the specific intensity fluctuation power spectra lies within -1.5 to -1.9 over a length scale range of 300 pc to 16 kpc across the entire galaxy sample. In their analysis, the slope of the power spectra for the galaxies NGC 5236 and NGC 6946 were -1.9 ± 0.2 between the baseline range of $0.6 - 6$ kλ and -1.6 ± 0.1 between the baseline range of $1.5 - 10.0$ kλ respectively. The slope for the galaxy NGC 5236 from our present result is consistant with the earlier result within three sigma uncertainties (see Table 3.3). The slope of the column density power spectrum of NGC 6946 measured in our analysis is significantly different from the slope of the intensity fluctuation power spectrum reported by Dutta et al. (2013). Note that, the visibility moment estimator of column density power spectrum supress the effect of the window function at lower baselines better than the legacy visibility correlation estimator used earlier. Hence, the slope reported in the present work can be considered as more accurate.

Our observation that both the column density and the velocity power spectra follow power laws over a large range of length scales strongly suggests the presence of large

scale turbulence cascade in these galaxies. Dutta et al. (2009) show that for the galaxy NGC 1058 the specific intensity power spectra steepens at a length scales lower than 1.5 kpc indicating a transition from the two-dimensional structure at the large scales to the three-dimensional structures at scales smaller than the scale-height of the galaxy. Block et al. (2010) and Combes (2012) observe similar trends in the power spectra of the dust emission in the LMC and the nearby galaxy M 33 respectively. The fact that we do not observe any such steepening down to a scale of 300 pc for NGC 5236 and 170 pc for NGC 6946, suggests that the scale heights of these galaxies are less than these respective scales. Patra (2020) estimate the 3D distribution of H I in seven nearby spiral galaxies. They show that for the galaxy NGC 6946 the scale height varies between ~ 100 pc to 300 pc. Bacchini et al. (2020) also mentioned a similar range of scale height variation. We conclude that the power spectra in both the galaxies here can be interpreted as arising from two-dimensional turbulence on the galaxy's disc.

For NGC 5236, our measurement gives the amplitude of column density fluctuation power spectrum as 4×10^{-4} at an angular scale of one steradian. For a power law slope of -1.23, the expected slope of the autocorrelation function of the column density distribution is -0.77. This corresponds to a standard deviation in column density fluctuation of 0.01 at a length scale of 11 kpc. Similarly, for NGC 6946, the power spectrum amplitude of 6.7×10^{-5} at one steradian and a slope of -0.96 gives rise to a value 0.01 for the standard deviation in the column density fluctuation at 5 kpc.

Table 3.4 compares our result on the slope of the H I column density and line of sight velocity power spectra in both galaxies with different theoretical models and simulations of turbulence for 2D disc. The Kolmogorov (1941) universal equilibrium theory for incompressible fluid turbulence predicts a velocity power spectrum with a slope of $-5/3$. The mathematical model by Burgers (1948) of compressive turbulence flow gives a slope of -2 for the velocity power spectrum. Federrath et al. (2009) perform numerical simulations

of compressible fluid turbulence and investigate the role of solenoidal and compressive forcing. They find for a pure solenoidal forcing the density and the velocity spectra assume slopes of -0.78 ± 0.06 and -1.86 ± 0.05 respectively. In the case of compressive forcing, the density power law slope is lower -1.44 ± 0.23, whereas the velocity spectrum slope is similar, -1.94 ± 0.05. Since the slope of the velocity fluctuation power spectra for two different forcing mechanism is rather similar, it is difficult to use the measured slope of the velocity fluctuation power spectrum to comment on the nature of turbulence forcing. However, the density fluctuation assumes different power law slopes for different forcing mechanism, making the slope of the density fluctuation power spectrum an indicator of the forcing mechanism.

Our measurement of the column density power spectrum slope of -1.23 for NGC 5236 suggests that most of the forcing behind the large scale ISM turbulence we probe here is compressive in nature. Using the phenomenological model of compressive turbulence by von Weizsäcker (1951), Fleck (1996) commented on the relation between the velocity and column density scaling index. Following this prescription, for a column density scaling of -1.23, we get a velocity power spectrum scaling of -1.92, consistent with the measured value here.

For the galaxy NGC 6946, the density power spectrum have a slope of -0.96. Using the relation between density and velocity power spectrum slope for compressible fluid turbulence, the velocity power spectrum slope for NGC 6946 is expected to be -2.01. This is consistant with our measured slope of -1.80 ± 0.13 within two sigma uncertainities. The column density slope of -0.96 is intermediate to the slopes found for compressive and solenoidal forcing by Federrath et al. (2009). We believe that the turbulence driving mechanism for NGC 6946 comes from a combination of compressive and solenoidal forcing. This believe is supported by the fact that NGC 6946 is found to have well designed

magnetic spiral arms located between optical arms (Beck et al., 1996). The following sections detail our inferences on various aspects of turbulences in these two galaxies.

3.5.1 Compressive turbulence in NGC 5236

Bournaud et al. (2010) have used numerical simulations to investigate the role of self-gravity, turbulence cascade and stellar feedback on the properties of the ISM in disc galaxies. They find the turbulence at a large scale is insensitive to the stellar feedback and mostly driven by gravitational instabilities. They conclude that the origin of the scale-invariant motions at the large scales can be result of a forward cascade originating from energy input through the spiral waves and other long range disturbances combined with an inverse cascade from the small scales. Elmegreen et al. (2003b) investigate the optical structure of M 33 at three different passbands. They conclude that the distribution of stars follows a fractal pattern generated by the background distribution of the turbulent ISM. Maier et al. (2016) use the sample of galaxies in the THINGS survey to investigate the relationship between turbulence and star formation. They conclude that the large scale turbulence is more likely to be driven by disc gravitational instabilities, density waves or bar streaming motions and is less likely to be the results of stellar activities. Ianjamasimanana et al. (2012) find that at the outer part of the galaxy's disc, the H I velocity dispersion has a broad component with velocity dispersion above ~ 5 km sec^{-1}, suggesting that the star formation is not the major player to drive the H I velocity dispersion favouring turbulence driving at the exteriors of the galaxy's disc. A similar conclusion is reached by the studies of Szotkowski et al. (2019) and Nestingen-Palm et al. (2017) on the Large Magellanic Cloud, where they infer that there is significant turbulence driving exists at the large scales from sources other than stellar feedback. Krumholz and Burkhart (2016) also show that it is more likely that the gravity is the source of the large scale ISM turbulence and wins over the stellar feedback. Elmegreen et al. (2003a) mention a turbulent origin of the spiral

structures in the galaxies. They compare the size of the largest structures with the critical Jeans length at that scale. They conclude that the self-gravity driven shear instabilities in large-scale generate the flocculent spiral arms. The energy of these instabilities drives turbulence at these scales which follow forward cascades to form smaller scale structures.

We find that the turbulent velocity fluctuations in the H I have a power of 88 (km sec^{-1})^2 at unit steradian. The corresponding power spectrum slope of -1.91 gives a power law slope of 0.09 in the autocorrelation function of the turbulent velocity fluctuations. Assuming the power law behaviours, at the scale of 6 kpc, the amplitude of the autocorrelation function of turbulent velocity fluctuation is ~ 160.5 (km sec^{-1})^2. This gives a turbulent velocity dispersion of ~ 31.2 km sec^{-1} at 6 kpc scales in the plane of the disc.

Considering a number density of 1 atom cm^{-3}, a velocity dispersion of 12.7 km sec^{-1} corresponds to a Jeans scale of ~ 8.0 kpc. In this work, the largest length scale to which we observe the power spectrum to follow power law is 11 kpc for the column density power spectra and 6 kpc for the velocity power spectra. Hence, the estimated Jeans scale is quite comparable to the largest scale to which we probe the power law velocity spectra. We believe this is an evidence that the gravitational instability drives the observed turbulence at ~ 6 kpc scales and maintains the large scale power spectra.

The galaxy NGC 5236 has an average inclination angle of 24°. A line of sight turbulent velocity dispersion of 12.7 km sec^{-1} at 6 kpc scales have a coherent component of 31 km sec^{-1} along the plane of the disc. We use the natural weighted moment 2 map of NGC 5236 from the THINGS archive [8] to estimate the radial variation of the line of sight H I velocity dispersion. Median velocity dispersion for NGC 5236 in elliptical annular regions is plotted against the galacto-centric distance in Figure 3.4. The ellipse position angle is chosen as the average position angle 225° of the galaxy's disc while the ellipticity is derived from the average inclination angle 24° (Tilanus and Allen, 1993; Walter et al., 2008). The vertical line in Figure 3.4 corresponds to the R_{25} of the galaxy (Walter et al.

[8] http://www.mpia.de/THINGS

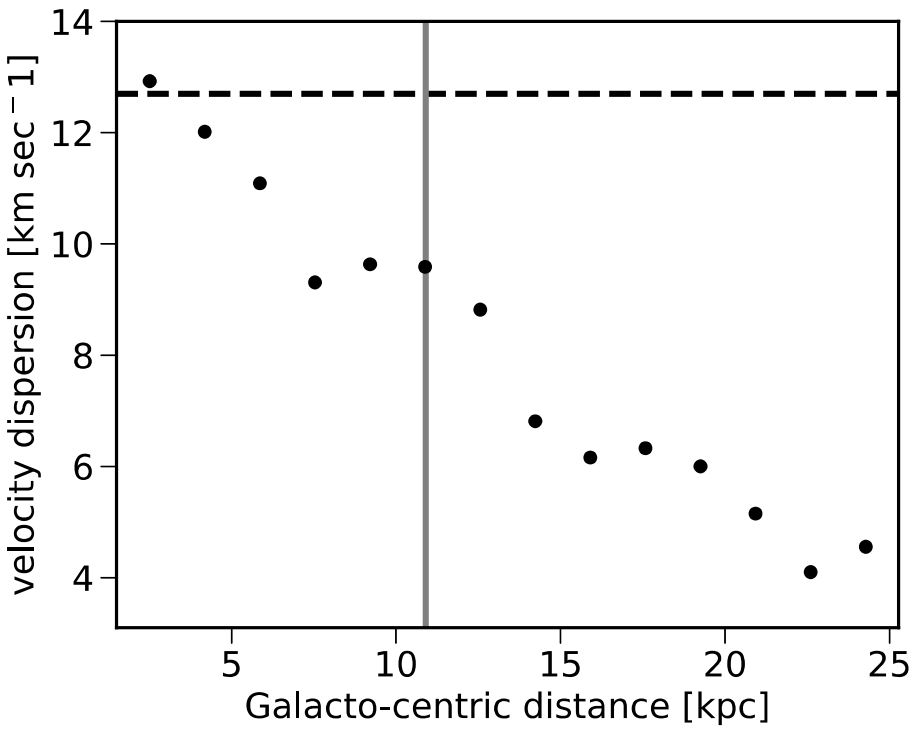

(a) NGC 5236

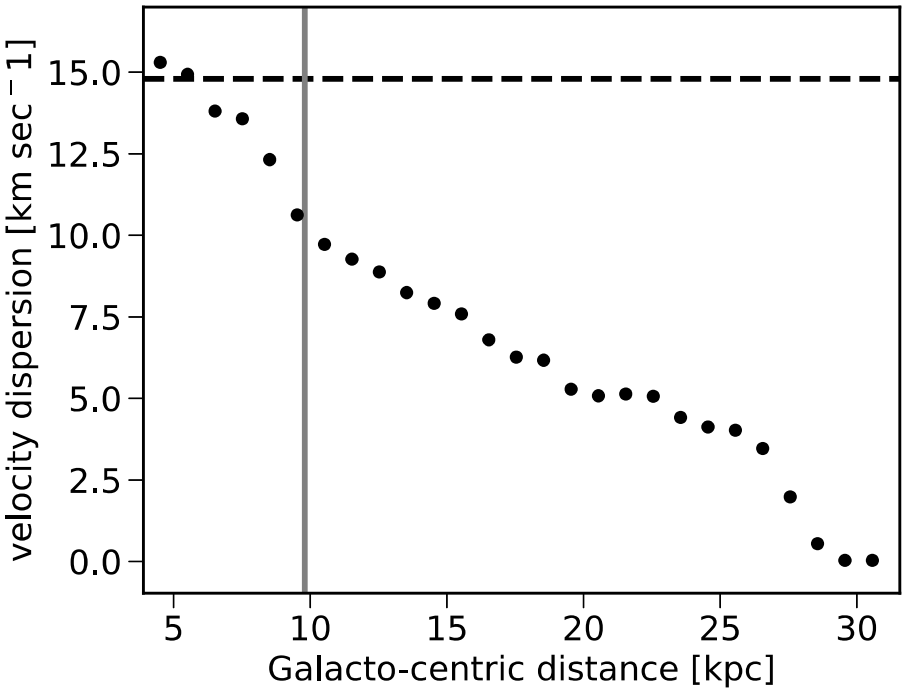

(b) NGC 6946

Fig. 3.4 Median velocity dispersion is plotted with galacto-centric radius (circles) for NGC 5236 and NGC 6946. The vertical line corresponds to the respective R_{25} of the galaxy. The horizontal line corresponds to the turbulence velocity dispersion at 6 kpc scale for both the galaxies.

(2008) table 1). The horizontal dashed line corresponds to the velocity dispersion at 6 kpc scale due to turbulence. The highest median line of sight velocity dispersion from the moment 2 map is approximately same as the line of sight turbulent velocity dispersion at 6 kpc scales. Using numerical simulation Bournaud et al. (2010) show that the power spectrum of the turbulent velocity dispersion from the off the disc component follows a power law till the thickness of the disc. They show that the on the disc components of the velocity power spectra continue to follow power laws at large scales and hence have higher velocity dispersion. The fact that the large scale coherent fluctuations in velocity we measure here, have a larger amplitude than the incoherent velocity dispersion, supports the simulation results.

Clearly, turbulence plays a significant role in the total velocity dispersion and is very significant to drive the dispersion beyond the stellar disc of the galaxy.

3.5.2 Nature of turbulence in NGC 6946

We have mentioned earlier that the turbulence energy for the galaxy NGC 6946 comes partly from solenoidal and partly from compressive forcing. The compressive forcing can arise from self gravity of the gas in large scales as discussed above for the case of NGC 5236. The known sources for solenoidal forcing in the galactic disks are the differential rotation generates shear and additional influence of magnetic field in the disk (Federrath et al., 2010; Sellwood and Balbus, 1999).

Large scale galactic magnetic fields are observed in several external spiral galaxies using radio synchrotron emission (Beck, 2013; Chyży and Buta, 2008; Krause, 2009). The typical field strength observed in spiral arms are $1 - 10\mu G$ (Sofue et al., 1986). Inter-arm magnetic fields, known as magnetic arms, are also observed. These magnetic arms are present in NGC 6946 (Beck et al., 1996). Beck (2007) reports multiple strong magnetic spiral arms ($\sim 20\mu G$) in NGC 6946 using radio polarization observation. On

their investigation of magnetic properties in this galaxy, the measured total magnetic energy density is found to be of similar order in the inner part of the galactic disc (< 2 kpc) compared to the outer part (up to 10 kpc). The ordered magnetic fields are found to present in NGC 6946 up to a radius of ~ 12 kpc and regular magnetic fields are detected up to ~ 15 kpc in Beck (2007) observations. These detected ordered fields are aligned along with the spiral structures which indicate the possible interaction of the gas in the arms with a magnetic field. Applying a non-turbulent dynamo model to the NGC 6946, through numerical studies Rohde et al. (1999) shows that observed magnetic structures in NGC 6946 can be well reproduced. These results suggest the observed magnetic structures are the result of turbulent dynamics in the disc. We are to conclude that the magnetic field of NGC 6946 has a major role to drive its large scale turbulence.

The line of sight turbulent velocity fluctuation power spectrum of NGC 6946 have a power law with amplitude 59 (km sec^{-1})^2 at unit steradian and a slope of -1.81. These corresponds to a turbulent velocity dispersion of 27.1 km sec^{-1} at 6 kpc scales in the plane of the disc. The bottom panel of figure 3.4 shows the radial variation of mean H I velocity dispersion in NGC 6946 as estimated from the moment 0 map. The vertical line marks R_{25} and the horizontal dashed line corresponds to the velocity dispersion at 6 kpc scale. Here also we see that the off the disc component of the velocity dispersion does not have the large velocity fluctuations as measured at scales higher than the thickness of the disc.

The energy input rate per unit area by the ISM turbulence can be estimated using $\epsilon = \frac{1}{2} \times (N_{\rm HI_0} \sigma_{\rm HI} m_{\rm HI}) \times (v^T)^2 \times v^T/L$, where $N_{\rm HI_0}$ is the average column density over the disc, $m_{\rm HI}$ is the mass of atomic hydrogen, $\sigma_{\rm HI}$ is the relative fluctuation of H I column density and v^T is the turbulent velocity fluctuation. The quantity $N_{\rm HI_0} \sigma_{\rm HI} m_{\rm HI}$ gives the mass of H I in turbulence per unit area, L/v^T gives the time scale of energy input. We find from the moment 0 map of the galaxy NGC 5236 and NGC 6946, the value of $N_{\rm HI_0}$ are 4×10^{20} and 3.7×10^{20} atoms cm^{-2} respectively. Considering the energy input scale is at

6 kpc, we find the turbulence energy inputs for these galaxies are $\sim 5 \times 10^{-10}$ ergs cm^{-2} sec^{-1} and $\sim 5.6 \times 10^{-10}$ ergs cm^{-2} sec^{-1} respectively. Taking the average energy released in a supernova of 10^{46} ergs as kinetic energy, a supernovae rate of one in 100 years, the average energy input rate by supernovae per unit area in this galaxy is about 3.5×10^{-10} ergs cm^{-2} sec^{-1}, quite comparable to the energy inputs in turbulence. This may explain, why in spite of different energy input mechanisms at different scales, the power spectra of the ISM turbulence follow a two-component power law over a large range of length scales.

3.6 Summary

In this chapter, the evidence for large scale turbulence cascade in two spiral galaxies are presented. The followings are the main findings of this work.

- The ISM is driven by compressive and solenoidal forcing at scales of 6 kpc.
- NGC 5236 shows compressive only driving for turbulence, whereas, NGC 6946 likely to have a combination of compressive and solenoidal driving for its large scale turbulence.
- The energy input rate by large scale turbulence is of the same order as that by the supernovae remnants at smaller scales.